Stability effects of finite difference methods on mathematical tumor growth model

Parisa Mosayebi, Dana Cobzas, Martin Jagersand, and Albert Murtha
University of Alberta
Edmonton, Canada
mosayebi@ualberta.ca, dana@cs.ualberta.ca, jag@cs.ualberta.ca, albertmu@cancerboard.ab.ca

Abstract

Numerical methods used for solving differential equations should be chosen with great care. Not considering numerical aspects such as stability, consistency and wellposed-ness results in erroneous solutions, which in turn will result in incorrect judgments. One of the most important aspects that should be considered is the stability of the numerical method.

In this paper, we discuss stability problems of some of the so far proposed finite difference methods for solving the anisotropic diffusion equation, a second order parabolic equation. This equation is used in a variety of applications in physics and image processing. Here, we focus on its usage in formulating brain tumor growth using the Diffusion Weighted Imaging (DWI) technique. Our study shows that the commonly used chain rule method to discretize diffusion equation is unstable. We propose a new 3D stable discretization method with its stability conditions to solve the diffusion equation. The new method uses directional discretization and forward differences. We also extend standard discretization method to 3D. The theoretical and practical comparisons of the three methods both on synthetic and real patient data show that while chain rule model is always unstable and standard discretization is unstable in theory, our proposed directional discretization is stable both in theory and practice.

1. Introduction

Partial Diffusion Equations (PDEs) are often used in medical imaging. A numerical method used to solve a PDE must be stable. This fact is more important in medical cases where not considering stability issues of numerical methods can cause incorrect judgments of medical doctors which in turn can result in developing incorrect treatment methods. Here, we discuss the stability issues of the 2nd order diffusion equation. This equation is used in a variety of applications including image enhancement, segmentation and filtering. But our application comes from brain tumor growth modeling. In this paper, we discuss the stability problems of some of the so far proposed numerical methods for solving the reaction-diffusion equation in the context of tumor growth prediction and we propose our new 3D stable method. Testing all the practical implications of the stability reveals that, of common finite difference schemes of diffusion models in the literature (considering anisotropy of tensor), one is almost always unstable, one is theoretically unstable but might be stable in practice and our method works on all test cases and only gets unstable if the condition is not satisfied.

Mathematical modeling of the tumor growth has a long history. The reaction-diffusion model, introduced by Murray [11], made a great change in growth modeling. The two main biological behaviours that are considered in this model are diffusion and proliferation. Diffusion illustrates the fact that tumor cells infiltrate into the surrounding brain tissue. Proliferation is a function representing a reactive behaviour that primarily accounts for tumor cell growth and death. Early works use an isotropic diffusion model that allows tumor cells to diffuse equally in all directions with the same speed for all tissues [4]. The experimental results of Giese et al. [1] established that tumor cells move faster in white matter than in gray matter. Swanson et al. [12], [13] incorporated this experimental fact to the growth model by multiplying the tensors in white matter with a scaling factor. This isotropic model, which results in spherical cell invasion, only simulates high-grade gliomas. Low-grade gliomas, which exhibit complex finger-like shapes, are not well described by an isotropic model. More recent approaches ([2], [8], [9], [3]) use anisotropic diffusion along white matter fibers as given by the diffusion tensors (from Diffusion Tensor Images-DTI) to simulate more complex tumors.

The two general numerical methods used to solve the reaction-diffusion equation in the context of tumor growth are finite elements or finite differences. Examples of models using finite-elements to solve anisotropic diffusion equation are [2], [10], [7]. But, the finite difference scheme is easier to implement and the pixel structure of digital images pro-

vides a natural regular grid. However, the anisotropic diffusion equation is a complex second order PDE and not any simple finite difference can solve it properly. In [9] and [3], this second order PDE is reformulated to simpler first order PDEs by using the concept of manifolds. But the solution of the equation is tumor delineation area or geodesic distances instead of the tumor cell density. In [8], anisotropic diffusion equation chain-rule expansion is directly solved by using chain rule expansion. In this paper, we prove that chain-rule expansion is an unstable solution. We compare the stability issues of three different 2D discretization methods. We further extend an stable one [14] with its aligned stability conditions to 3D to solve the anisotropic tumor growth diffusion equation and find the tumor cell density. We finally compare the 3D chain-rule model with our model on real patient data.

2. Numerical Solutions of Anisotropic Diffusion PDEs

The reaction-diffusion equation, proposed by Murray [11] *et al.*, to model the tumor growth has the following general format:

$$\begin{cases} \frac{\partial u}{\partial t} = \underbrace{\operatorname{div}(\mathbf{D}\nabla u)}_{\text{DiffusionTerm}} + \underbrace{f(u)}_{\text{ProliferationTerm}} - \underbrace{T(u)}_{\text{Treatmentlaw}} \\ \mathbf{D}\nabla u.\vec{n}_{\partial\Omega} = 0 \end{cases} \tag{1}$$

where the second row defines the Neumann boundary conditions; Ω shows the domain (3D image) and $\partial\Omega$ is its boundary, D is the diffusion tensor and u is the normalized tumor cell density ($u \in [0,1]$). The simplest choice for the proliferation term is the exponential format which uses constant growth rate of glioma cells (ρ). Here, we use exponential proliferation and we do not consider the treatment planning. Therefore, the whole equation is simplified as:

$$\begin{cases} \frac{\partial u}{\partial t} = \operatorname{div}(\mathbf{D}.\nabla u) + \rho u \\ \mathbf{D}\nabla u.\vec{n}_{\partial\Omega} = 0 \end{cases} \tag{2}$$

To find the rate of change of tumor cell densities in time, we need to solve equation 2 using numerical methods.

2.1. Implementing the reaction-diffusion equation, Numerical issues

According to standard textbook definition (e.g. [6], in studying differential equations, a numerical method is said to be *stable* if small perturbations in the input data or the ones that occur during computation do not cause the resulting numerical solution to diverge away without bound. In other words, a numerical method is *stable* if the numerical solution at any arbitrary but fixed time t remains bounded [6].

To access the stability issues of discretizing the reaction-diffusion equation, we first consider only the diffusion term. The diffusion term has the general format of:

$$\begin{aligned} \frac{\partial u}{\partial t} &= \operatorname{div}(D\nabla u) = \operatorname{div}\left(\begin{bmatrix} a & b \\ b & c \end{bmatrix}\begin{bmatrix} \frac{\partial u}{\partial x} \\ \frac{\partial u}{\partial y} \end{bmatrix}\right) \\ &= \frac{\partial(a\frac{\partial u}{\partial x})}{\partial x} + \frac{\partial(b\frac{\partial u}{\partial y})}{\partial x} + \frac{\partial(b\frac{\partial u}{\partial x})}{\partial y} + \frac{\partial(c\frac{\partial u}{\partial y})}{\partial y} \end{aligned} \tag{3}$$

Discretization of the right hand side of the diffusion equation using finite differences results in a semi-discrete problem. To assess the well-posedness of the semidiscrete problem, let us first define the semidiscrete class of diffusion problems (P_s) following Weickert [14]:

(P_s) Let $f \in \Re^N$. Find a function $u \in C^1([0,\infty), \Re^N)$ that satisfies an initial value problem of type

$$\frac{\partial u}{\partial t} = A(u)u,$$
$$u(0) = f,$$

where $A = (a_{ij})$ has the following properties:

(S1) Lipschitz-continuity of $A \in C(\Re^N, \Re^{N\times N})$ for every bounded subset of $\Re^N$

(S2) symmetry:
$a_{ij}(u) = a_{ji}(u) \quad \forall i,j \in J, \quad \forall u \in \Re^N,$

(S3) vanishing row sums:
$\sum_{j\in J} a_{ij}(u) = 0 \quad \forall i \in J, \quad \forall u \in \Re^N,$

(S4) nonnegative off-diagonals:
$a_{ij}(u) \geq 0 \quad \forall i \neq j, \quad \forall u \in \Re^N$

2.1.1 Theorem of well-posedness, extremum principle for semidiscrete problems

For every $T > 0$ the problem (P_s) has a unique solution $u(t) \in C^1([0,T], \Re^N)$. The solution depends continuously on the initial value and the right-hand side of the ODE system, and it satisfies the extremum principle

$$a \leq u_i(t) \leq b \quad \forall i \in J, \quad \forall t \in [0,T], \tag{4}$$

where

$$\begin{aligned} a &:= \min_{j\in J} f_j, \\ b &:= \max_{j\in J} f_j \end{aligned} \tag{5}$$

This theorem is proved in [14]. Based on this theory, if a semi-discrete problem belongs to (P_s) class, it will have a unique stable solution. For the diffusion equation, since D is a positive semidefinite matrix (S1) to (S3) are satisfied. The only remained term that needs to be satisfied is the nonnegativity term (S4). If (S4) is not satisfied, the numerical method gets unstable. However, satisfying (S4)

$\frac{-b_{i,j}}{2h_1h_2}$	$\frac{b_{i+1,j}-b_{i-1,j}}{4h_1h_2}$ $+\frac{c_{i,j+1}-c_{i,j-1}}{4h_2^2}$ $+\frac{c_{i,j}}{h_2^2}$	$\frac{b_{i,j}}{2h_1h_2}$
$\frac{a_{i,j}}{h_1^2}$ $-\frac{a_{i+1,j}-a_{i-1,j}}{4h_1^2}$ $-\frac{b_{i,j+1}-b_{i,j-1}}{4h_1h_2}$	$-\frac{2a_{i,j}}{h_1^2}-\frac{2c_{i,j}}{h_2^2}$	$\frac{a_{i,j}}{h_1^2}$ $+\frac{a_{i+1,j}-a_{i-1,j}}{4h_1^2}$ $+\frac{b_{i,j+1}-b_{i,j-1}}{4h_1h_2}$
$\frac{b_{i,j}}{2h_1h_2}$	$-\frac{b_{i+1,j}-b_{i-1,j}}{4h_1h_2}$ $-\frac{c_{i,j+1}-c_{i,j-1}}{4h_2^2}$ $+\frac{c_{i,j}}{h_2^2}$	$\frac{-b_{i,j}}{2h_1h_2}$

Table 1. Chain-Rule 2D stencil; Discretization with this stencil is not guaranteed to be stable since all stencil elements can get negative

is not an easy task that cannot be solved with simple discretization methods. Here, we explain how three different 2D discretization methods affect the (S4) condition.

2.1.2 Chain-rule discretization method

The simplest way to discretize a second order derivative is to use Chain-Rule discretization method. In the chain-rule method, the derivatives of 3 are defined as:

$$\partial\left(a\frac{\partial u}{\partial x}\right)=\frac{\partial a}{\partial x}\frac{\partial u}{\partial x}+a\frac{\partial^2 u}{\partial x^2} \tag{6}$$

and by using the forward and centered finite difference schemes of the following format, we will end up in a stencil with the format of Table 1.

$$\begin{array}{l}\frac{\partial u}{\partial x}=\frac{u_{i+1,j}-ui,j}{2h_1}\\ \frac{\partial^2 u}{\partial x^2}=\frac{u_{i+1,j}-2ui,j+u_{i,j+1}}{h_1^2}\end{array} \tag{7}$$

Satisfying (S4) requires that all non-centered elements of Table 1 be non-negative. Positive semi-definiteness of the tensor D guarantees that diagonal elements of the tensor (a and c) are nonnegative. But this fact is not helpful in case of chain-rule discretization and all the elements of the stencil of the table 1 can violate the nonnegativity even the ones containing only a and c coefficients. Subsequently, chain-rule method violates the stability issues. This method was extended to 3D in [8]. Obviously the 3D extension is also unstable.

2.1.3 Standard discretization method

Standard discretization method is another method used by Weickert [14] in which, forward-backward and mixed term

$\frac{-b_{i-1,j}-b_{i,j+1}}{4h_1h_2}$	$\frac{c_{i,j+1}+c_{i,j}}{2h_2^2}$	$\frac{b_{i+1,j}+b_{i,j+1}}{4h_1h_2}$
$\frac{a_{i-1,j}+a_{i,j}}{2h_1^2}$	$-\frac{a_{i-1,j}+2a_{i,j}+a_{i+1,j}}{2h_1^2}$ $-\frac{c_{i,j-1}+2c_{i,j}+c_{i,j+1}}{2h_2^2}$	$\frac{a_{i+1,j}+a_{i,j}}{2h_1^2}$
$\frac{b_{i-1,j}+b_{i,j-1}}{4h_1h_2}$	$\frac{c_{i,j-1}+c_{i,j}}{2h_2^2}$	$\frac{-b_{i+1,j}+b_{i,j-1}}{4h_1h_2}$

Table 2. Standard 2D stencil; Discretization with this stencil is not guaranteed to be stable since the diagonal boundary elements of the stencil can become negative

differences are obtained by:

$$\begin{array}{l}\frac{\partial(a\frac{\partial u}{\partial x})}{\partial x}=\\ \quad\frac{1}{h_1}\left(\frac{a_{i+1,j}+a_{i,j}}{2}\frac{u_{i+1,j}-u_{i,j}}{h_1}-\frac{a_{i,j}+a_{i-1,j}}{2}\frac{u_{i,j}-u_{i-1,j}}{h_1}\right)\\ \frac{\partial(b\frac{\partial u}{\partial y})}{\partial x}=\\ \frac{1}{2h_1}\left(b_{i+1,j}\frac{u_{i+1,j+1}-u_{i+1,j-1}}{2h_2}-b_{i-1,j,k}\frac{u_{i-1,j+1}-u_{i-1,j-1}}{2h_2}\right)\end{array} \tag{8}$$

This standard discretization results in a stencil of the format of Table 2. Off-diagonal elements of the stencil are nonnegative, since a and c are nonnegative but the nonnegativity of the whole stencil cannot be guaranteed since the b values have undefined sign.

2.1.4 Non-negative discretization method

In standard method, the discretization of the mixed term derivatives as defined in equation 8 produces negatives terms in the stencil. To solve this problem, Weickert [14] suggested calculating the derivatives in some newly defined directions in addition to the original directions (x, y). In 2D, the new directions are the diagonal directions of the 3×3-stencil. The mixed term derivatives in equation 3 are therefore replaced by directional derivatives. To obtain a nonnegative stencil, it is enough to find the conditions under which the stencil weights of the new directions are nonnegative.
Weickert [14] proved the existence of such a nonnegative second-order FD discretization on a $(2m+1)\times(2m+1)$ stencil for $\mathrm{div}(D\nabla u)$. He also calculated the elements of the stencil and the stability conditions for a 3×3 stencil. We extend this method to 3D case.

2.1.5 3D Non-negative discretization method

In order to solve the tumor growth anisotropic diffusion, we need to extend one stable discretization method to 3D. Pre-

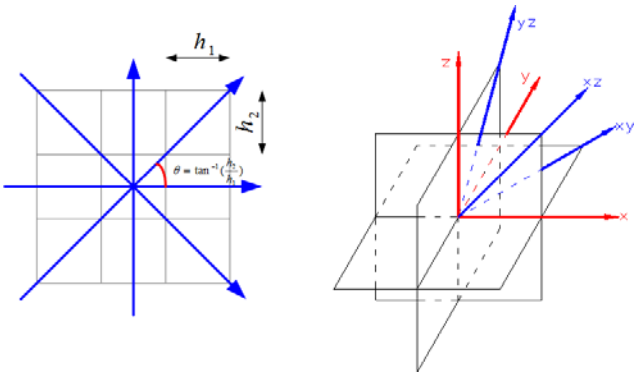

Figure 1. 2D and 3D Stencil. Left: 2D stencil with the four principal directions. Right: Three main planes of the 3D stencil with the six principal orientations

viously, the chain-rule method was extended to 3D for this mean [8]. However, as we proved, this method is unstable even for the 2D case. In this paper, we extend the conditionally stable method proposed by Weickert [14] to 3D. For 3D extension, we consider the 3D stencil as a combination of three 2D stencils in xy, yz and xz planes. In each plane, we have a 3×3 stencil. The "boundary pixels" of this stencil define four principal orientations $\beta_i \in (-\frac{\pi}{2}, \frac{\pi}{2}]$ corresponding to angles $\left(-\arctan\left(\frac{h_2}{h_1}\right),\ 0,\ \arctan\left(\frac{h_2}{h_1}\right),\ \frac{\pi}{2}\right)$. Figure 1-left shows a 3×3-stencil with the principal directions. We can define a partion of $(-\frac{\pi}{2}, \frac{\pi}{2}]$ into two subintervals:

$$(-\frac{\pi}{2}, \frac{\pi}{2}] = (-\frac{\pi}{2}, 0] \cup (0, \frac{\pi}{2}] = I_1 \cup I_{-1}$$

In the 3D coordinate system, each orientation is shown with three angles θ_x, θ_y and θ_z which define the angles to the three coordinate axes x, y and z. The directional splitting of the diffusion equation in 3D results in:

$$\begin{aligned}
&\mathrm{div}(D\nabla u) = \\
&\partial e_{\beta_x}(\alpha_x e_{\beta_x} u) + \partial e_{\beta_y}(\alpha_y e_{\beta_y} u) + \partial e_{\beta_z}(\alpha_z e_{\beta_z} u) + \\
&\partial e_{\beta_{xy}}(\alpha_{xy} e_{\beta_{xy}} u) + \partial e_{\beta_{-xy}}(\alpha_{-xy} e_{\beta_{-xy}} u) + \\
&\partial e_{\beta_{xz}}(\alpha_{xz} e_{\beta_{xz}} u) + \partial e_{\beta_{-xz}}(\alpha_{-xz} e_{\beta_{-xz}} u) + \\
&\partial e_{\beta_{yz}}(\alpha_{yz} e_{\beta_{yz}} u) + \partial e_{\beta_{-yz}}(\alpha_{-yz} e_{\beta_{-yz}} u) +
\end{aligned} \tag{10}$$

where e_{β_i} denotes the stencil direction and α_i shows the coefficient along the corresponding direction. A nonnegative discrete method is obtained if α_i coefficients are nonnegative. In the rest of this section, we will find conditions under which directional coefficients remain nonnegative. First, for simplicity and also in order to use subsequent indices, let us define

$$\begin{aligned}
&\phi_0 := \beta_x, \phi_1 := \beta_y, \phi_2 := \beta_z \\
&\phi_3 := \beta_{xy}, \phi_4 := \beta_{xz}, \phi_5 := \beta_{yz}. \\
&\gamma_0 := \alpha_x, \gamma_1 := \alpha_y, \gamma_2 := \alpha_z \\
&\gamma_3 := \alpha_{xy}, \gamma_4 := \alpha_{xz}, \gamma_5 := \alpha_{yz}
\end{aligned} \tag{11}$$

In each plane, there is only one diagonal direction that has a positive coefficient and the other diagonal direction has a zero coefficient. For example, in xy plane, if α_{xy} is positive then α_{-xy} is zero and vise a versa. Hence, for simplicity, we can keep only one diagonal direction in each plane and we will keep the one in I_1 partition (between $(0, \frac{\pi}{2}]$). When the coefficient for one diagonal direction is defined, it will be easy to find the other one from it. Figure 1-right shows the three planes of a $3 \times 3 \times 3$-stencil with the defined six principal directions.

By substituting new coefficients of equation 11 in equation 10, we will obtain equation 9. By solving equation 9, γ values are defined as:

$$\begin{aligned}
\gamma_0 &= a - c\frac{\cos\phi_{4x}}{\cos\phi_{4z}} - b\frac{\cos\phi_{3x}}{\cos\phi_{3y}} \\
\gamma_1 &= d - e\frac{\cos\phi_{5y}}{\cos\phi_{5z}} - b\frac{\cos\phi_{3y}}{\cos\phi_{3x}} \\
\gamma_2 &= f - e\frac{\cos\phi_{5z}}{\cos\phi_{5y}} - c\frac{\cos\phi_{4z}}{\cos\phi_{4x}} \\
\gamma_3 &= \frac{b}{\cos\phi_{3x}\cos\phi_{3y}} \\
\gamma_4 &= \frac{c}{\cos\phi_{4x}\cos\phi_{4z}} \\
\gamma_5 &= \frac{e}{\cos\phi_{5y}\cos\phi_{5z}}
\end{aligned} \tag{12}$$

To have a nonnegative discretization, the coefficients γ_0 to γ_5 must be nonnegative. If the grid sizes are h_1, h_2 and h_3, the coefficients for all the nine directions are defined as:

$$\begin{aligned}
\gamma_x &= a - |c|\tfrac{h_1}{h_3} - |b|\tfrac{h_1}{h_2} \geq 0 \\
\gamma_y &= d - |e|\tfrac{h_2}{h_3} - |b|\tfrac{h_2}{h_1} \geq 0 \\
\gamma_z &= f - |e|\tfrac{h_3}{h_2} - |c|\tfrac{h_3}{h_1} \geq 0 \\
\gamma_{xy} &= (|b| + b).\tfrac{h_1^2+h_2^2}{h_1h_2} \geq 0 \\
\gamma_{-xy} &= (|b| - b).\tfrac{h_1^2+h_2^2}{h_1h_2} \geq 0 \\
\gamma_{xz} &= (|c| + c).\tfrac{h_1^2+h_3^2}{h_1h_3} \geq 0 \\
\gamma_{-xz} &= (|c| - c).\tfrac{h_1^2+h_3^2}{h_1h_3} \geq 0 \\
\gamma_{yz} &= (|e| + e).\tfrac{h_2^2+h_3^2}{h_2h_3} \geq 0 \\
\gamma_{-yz} &= (|e| - e).\tfrac{h_2^2+h_3^2}{h_3h_3} \geq 0
\end{aligned} \tag{13}$$

From equation 13 we can define the condition of the tensor for a nonnegative discretization:

$$\begin{aligned}
a &\geq |c|\tfrac{h_1}{h_3} + |b|\tfrac{h_1}{h_2} \\
d &\geq |e|\tfrac{h_2}{h_3} + |b|\tfrac{h_2}{h_1} \\
f &\geq |e|\tfrac{h_3}{h_2} + |c|\tfrac{h_3}{h_1}
\end{aligned} \tag{14}$$

Finally, we can find the nonnegative weights of the stencil by replacing the coefficients of equation 13 in equation 10 and by considering the directional step sizes (e.g. $\sqrt{h_1^2 + h_2^2}$ for the xy direction). The final stencil is given

$$
\begin{aligned}
div(D\nabla U) &= div\left(\begin{pmatrix} a & b & c \\ b & d & e \\ c & e & f \end{pmatrix}\nabla u\right) = \sum_{i=0}^{5}\frac{\partial}{\partial e_{\phi_i}}(\gamma_i\frac{\partial}{\partial e_{\phi_i}}) \\
&= \frac{\partial}{\partial x}\sum_{i=0}^{5}\cos\phi_{ix}(\gamma_i(u_x\cos\phi_{ix}+u_y\cos\phi_{iy}+u_z\cos\phi_{iz})) \\
&+ \frac{\partial}{\partial y}\sum_{i=0}^{5}\cos\phi_{iy}(\gamma_i(u_x\cos\phi_{ix}+u_y\cos\phi_{iy}+u_z\cos\phi_{iz})) \\
&+ \frac{\partial}{\partial z}\sum_{i=0}^{5}\cos\phi_{iz}(\gamma_i(u_x\cos\phi_{ix}+u_y\cos\phi_{iy}+u_z\cos\phi_{iz})) \\
&= div\left(\begin{pmatrix} \sum_{i=0}^{5}\gamma_i\cos^2\phi_{ix} & \sum_{i=0}^{5}\gamma_i\cos\phi_{ix}\cos\phi_{iy} & \sum_{i=0}^{5}\gamma_i\cos\phi_{ix}\cos\phi_{iz} \\ \sum_{i=0}^{5}\gamma_i\cos\phi_{iy}\cos\phi_{ix} & \sum_{i=0}^{5}\gamma_i\cos^2\phi_{iy} & \sum_{i=0}^{5}\gamma_i\cos\phi_{iy}\cos\phi_{iz} \\ \sum_{i=0}^{5}\gamma_i\cos\phi_{ix}\cos\phi_{iz} & \sum_{i=0}^{5}\gamma_i\cos\phi_{iy}\cos\phi_{iz} & \sum_{i=0}^{5}\gamma_i\cos^2\phi_{iz} \end{pmatrix}\nabla u\right)
\end{aligned} \tag{9}
$$

in Table 4 in the Appendix (Section 4). Using this stencil guarantees a stable spatial discretization assuming equation 14 is satisfied.

3. Experiments

In this section, we evaluate the stability issues of three different discretization methods for solving the second order parabolic PDE of the anisotropic diffusive tumor growth model. These models include chain-rule, standard and nonnegative discretization models. To evaluate the stability, we first test the introduced methods on 2D and 3D synthetic test cases and then evaluate them on real DTI data of patients. Finally, we provide visual examples of both stable and unstable cases.

3.1. Test on Synthetic Data

To test the degree of stability of each method, we made several 2D examples with different degrees of complexity. The first example is a 64×64 image with a circle in the middle corresponding to tumor at initial time as shown in figure 2. The pixel values corresponding to normalized tumor cell density are 1 inside the circle and 0 outside. The image values inside the circle remain 1 in all iterations representing the boundary condition. The strict max-min stability condition states that the normalized tumor cell density should be between 0 and 1 in all iterations. A less strict stability condition is to check only the maximum stability. If the proliferation rate is more than zero, we consider a free boundary problem meaning that once the tumor cell density of a voxel reaches the value 1, the voxel will be added to the boundary in subsequent iterations. We also need to make a diffusion tensor image corresponding to this image. The shape of the tensors are symbolically shown in figure 2. Diffusion tensor image includes a ribbon of tensors with the anisotropy parallel to x direction and another ribbon of tensors in the y direction. The tensors in the middle are the summation of both ribbons and are isotropic. The rest of the image is covered with very small isotropic tensors. In choosing the

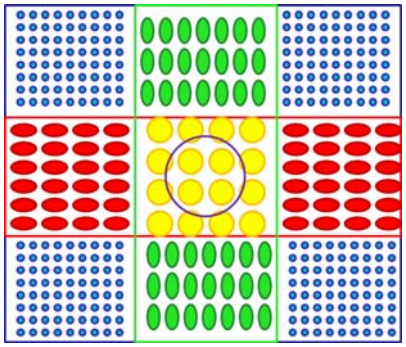

Figure 2. Tensor template for a 2D sample synthetic model. The simulation starts from the circle in the middle that is the symbol of tumor at initial time. Tensor shapes show the size and the degree of isotropy in different locations

values of the tensors we should always notice that tensors should be symmetric positive definite. The simplest case is where $b = 0$ for all tensors and the tensors satisfy stability condition ($cond(D) > 5.8$ as defined in [14]). Even for this simple model, the chain rule discretization model always simply becomes unstable. Figure 3 illustrates the result of applying chain rule and nonnegative models on this simple test case.

We eventually made the test cases more complicated. We found out that in most practical applications both standard and nonnegative discretization methods are maximally stable. The minimum values decreased below zero but they remained bounded. So we tried to find an example where the maximum stability was also ruined with these models. Finally, by using a complicated model with random tensor

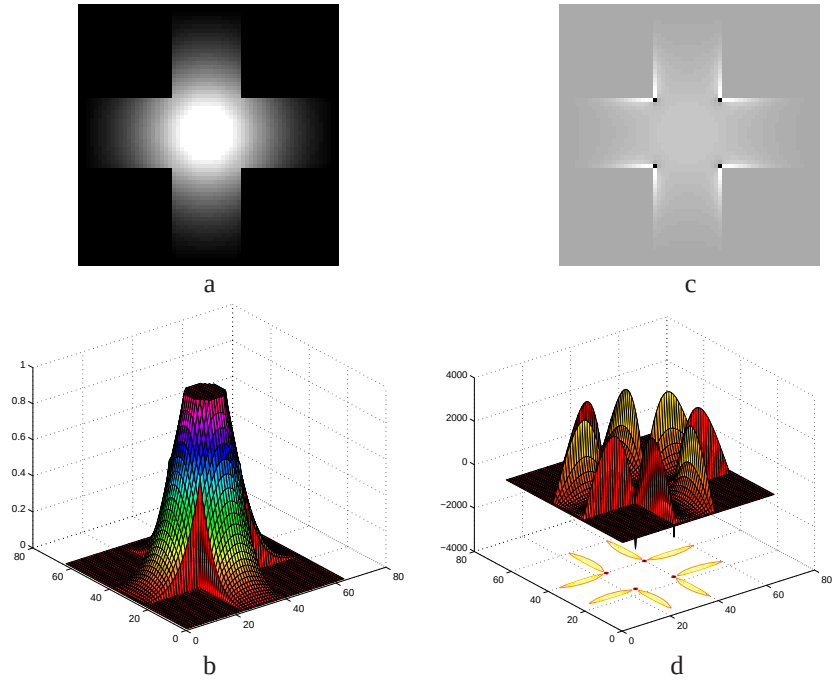

Figure 3. The results of applying two numerical methods on a simple test case. a and b) 2D and 3D representation of Nonnegative method results, this stable example nicely shows the diffusive nature of the growth. The pixel values remain in 0-1 range and do not violate the max-min stability issue c and d) 2D and 3D representation of Chain rule results, the white and black pixels on the edges of the ribbon in (c) correspond respectively to the pixels with very high and low intensities that destroy the max-min stability which is shown by high peaks and valleys in (d). Note how the intensity values are far from the 0-1 range in (d)

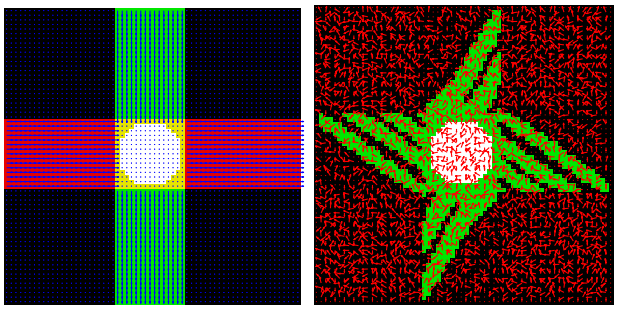

Figure 4. Synthetic test templates with first eigenvectors of corresponding diffusion tensors plotted on them; Left: a simple model of 2. This model can only make chain-rule model unstable. Right: A complicated test model where tensors in the green area are larger than the rest of the image which produces a high gradient field in tensor values. Also directions of tensors are completely random as red arrows show. All discretization models are even maximally unstable in this example

distribution on a high gradient irregular shape (instead of rectangular ribbons), we could achieve instability in these methods with $cond(D) > 5.8$. Figure 4 shows the two test models. Note that the $cond(D) > 5.8$ ruins the stability condition for the nonnegative model.

3.2. Test on Real Data

We extended all three mentioned discretization models to 3D to test the glioma growth model on real patient data. We used MRI and DTI data from clinical scans of patients with glioma.[1] DTI data has a resolution of $128 \times 128 \times 60$ while MRI data has a resolution of $512 \times 512 \times 21$. Typically at least one or two DTI data is acquired after radiation and the rest of the scans are conventional MRI images (T2, T1, FLAIR). For validation, we grow the tumor from *time1* (first DTI scan acquired after radiation) to approximately its size at *time2* (3-6 months later) and then compare the result of our model with the actual growth. The growth starts from the manually segmented visible high signal on DWI-b0 (Fig. 5, red contour). We extract diffusion tensors using ExploreDTI [5] from diffusion weighted images. More details on data preprocessing steps and real data experiments can be fined in [3].

For the initial value condition, we chose value $u = 1$ (corresponding to 100% tumor cells) for the voxels inside the visible part of the tumor in *time1* and $u = 0$ (corresponding to no tumor cells) for the rest. The free boundary condition indicates that the voxels with value $u = 1$ keep their value $u = 1$ during all iterations, based on the fact that once a voxel area of the brain is saturated with tumor cells, the number of cells cannot add up. We tested these models on four different real patient data sets, which is a relatively large number in comparisons with previous attempts in the literature where at most one real test case is used. The re-

[1]The data collection protocol was approved by REB and the patients that have provided an informed consent.

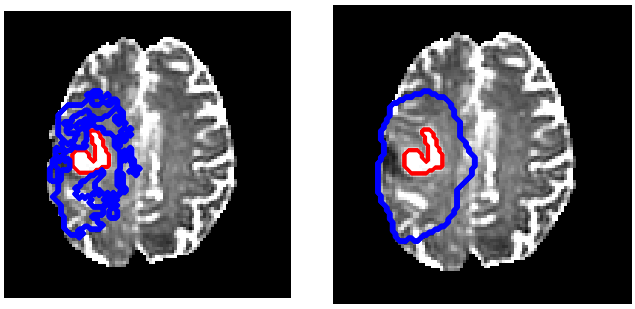

Figure 5. Test of anisotropic diffusive model on real DTI data of patients with glioma. Red contour shows the starting area of the growth simulation. Left) Result of applying chain-rule model, the blue contours show the result of an inhomogeneous growth caused by an unstable model. Right) Result of applying nonnegative discretization method. The homogenous contour indicates a stable growth.

Method	Theory	In practice
Chain-rule	unstabe	unstable
Standard	unstable	Stable (3 of 4 cases)
Nonnegative	Conditionally stable	Stable (3 of 4 cases)

Table 3. Comparison of the three discusses discretization methods in theory and in practice

sults show that the chain-rule model becomes unstable very soon in all cases. Standard and nonnegative methods remain stable in three cases if we just consider max stability, not max-min stability.

Fig. 5-right shows a sample of nonnegative method that remains stable through the simulation process. The tumor starts its growth from the red margin and keeps growing to a certain volume. The growth area remains homogenous. Fig. 5-left shows the result of applying chain-rule method to the same data. The instability results in a non-homogenous area that is seen as irregular blue contours. We conclude that, if we only take into account the max stability and not the max-min stability, Weickert's methods remain stable on real data without post processing on tensors. But a post processing that increases the degree of anisotropy will consequently increase the tensor condition number and destroy the stability condition defined in equation 14. The comparison results is concluded in Table 3. The reason that in practice the nonnegative model becomes unstable in one of the four real test cases is that the condition 14 is not satisfied in that case.

4. Conclusion

In this paper, we proposed a new 3D finite differences method for discretization of the anisotropic diffusion equation, a second order hyperbolic PDE. We proposed this model to tackle the instability problem of the previously used state of the art numerical methods in the context of tumor growth. Although we used anisotropic diffusion to model the infiltration of tumor cells into surrounding brain tissue, this equation has many other applications in physics and image processing. Therefore, a 3D stable numerical solution for this PDE is also very helpful for other applications. In this paper, after defining the general stability term, we proved that a simple chain rule method and also standard discretization methods violates this term. Instead, we proposed the extension of directional discretization to 3D and proved that it satisfies the stability term under certain conditions. We evaluated all three methods on synthetic and real patients' DWI data. We can conclude that in practice, chain rule method easily gets unstable. Standard discretization is mostly maximally stable though it is theoretically unstable. And the directional discretization (nonnegative) method is both theoretically and practically stable if the condition is satisfied.

References

[1] G. A., L. Kluwe, B. Laube, H. Meissner, M. Berens, and M. Westphal. Migration of human glioma cells on myelin. *Neurosurgery*, 38:755–764, 1996. 1

[2] O. Clatz, M. Sermesant, P. Bondiau, H. Delingette, S. Warfield, G. Malandain, and N. Ayache. Realistic simulation of the 3d growth of brain tumors in MR images coupling diffusion with mass effect. *IEEE Transactions on Medical Imaging*, 24(10):1334–1346, 2005. 1

[3] D. Cobzas, P. Mosayebi, A. Murtha, and M. Jagersand. Tumor invasion margin on the riemannian space of brain fibers. In *MICCAI*, 2009. 1, 2, 6

[4] G. Cruywagen, D. Woodward, P. Tracqui, G. Bartoo, J. Murray, and E. Alvord. The modeling of diffusive tumours. *J. Biol. Sys*, 3:937–945, 1995. 1

[5] ExploreDTI. http://www.exploredti.com/. 6

[6] M. Heath. *Scientific Computing, An Introdutory Survey*. McGraw-Hill, 2002. 2

[7] C. Hogea, F. Abraham, G. Biros, and C. Davatzikos. A framework for soft tissue simulations with applications to modeling brain tumor mass-effect in 3d images. In *MICCAI*, 2006. 1

[8] S. Jbabdi, E. Mandonnet, H. Duffau, L. Capelle, K. Swanson, M. Pelegrini, R. Guillevin, and H. Benali. Simulation of anisotropic growth of low-grade gliomas using dif. tensor imag. *Magnetic Resonance in Medicine*, 54:616–624, 2005. 1, 2, 3, 4

[9] E. Konukoglu, O. Clatz, B. Menze, M.-A. Weber, B. Stieltjes, E. Mandonnet, H. Delingette, and N. Ayache. Image guided personalization of reaction-diffusion type tumor growth models using modified anisotropic eikonal equations, Accepted to be published 2009. 1, 2

[10] A. Mohamed and C. Davatzikos. Finite element modeling of brain tumor mass-effect from 3d medical images. In *MICCAI*, pages 400–408, 2005. 1

[11] J. Murray. *Mathematical Biology*. Springer-Verlag, Heidelberg, 1989. 1, 2

[12] K. Swanson, E. Alvord, and J. Murray. A quantitative model for differential motility of gliomas in grey and white matter. *Cell Proliferation*, 33:317–329, 2000. 1

[13] K. Swanson, E. Alvord, and J. Murray. Virtual brain tumors (gliomas) enhance the reality of medical imaging and highlight inadequacies of current therapy. *British Journal of Cancer*, 85:14–18, 2002. 1

[14] J. Weickert. *Anisotropic Diffusion in Image Processing*. ECMI Series, Teubner-Verlag, Stuttgart, 1998. 2, 3, 4, 5

k-1

j+1		$\frac{\lvert e_{i,j+1,k-1}\rvert - e_{i,j+1,k-1}}{4h_2h_3}$ $+ \frac{\lvert e_{i,j,k}\rvert - e_{i,j,k}}{4h_2h_3}$	
j	$\frac{\lvert c_{i-1,j,k-1}\rvert + c_{i-1,j,k-1}}{4h_1h_3}$ $+ \frac{\lvert c_{i,j,k}\rvert + c_{i,j,k}}{4h_1h_3}$	$\frac{f_{i,j,k-1}+f_{i,j,k}}{2h_3^2} - \frac{\lvert c_{i,j,k-1}\rvert + \lvert c_{i,j,k}\rvert}{2h_1h_3} - \frac{\lvert e_{i,j,k-1}\rvert + \lvert e_{i,j,k}\rvert}{2h_2h_3}$	$\frac{\lvert c_{i+1,j,k-1}\rvert - c_{i+1,j,k-1}}{4h_1h_3}$ $+ \frac{\lvert c_{i,j,k}\rvert - c_{i,j,k}}{4h_1h_3}$
j-1		$\frac{\lvert e_{i,j-1,k-1}\rvert + e_{i,j-1,k-1}}{4h_2h_3}$ $+ \frac{\lvert e_{i,j,k}\rvert + e_{i,j,k}}{4h_2h_3}$	
	i-1	i	i+1

k

j+1	$\frac{\lvert b_{i-1,j+1,k}\rvert - b_{i-1,j+1,k}}{4h_1h_2}$ $+ \frac{\lvert b_{i,j,k}\rvert - b_{i,j,k}}{4h_1h_2}$	$\frac{d_{i,j+1,k}+d_{i,j,k}}{2h_2^2} - \frac{\lvert b_{i,j+1,k}\rvert + \lvert b_{i,j,k}\rvert}{2h_1h_2} - \frac{\lvert e_{i,j+1,k}\rvert + \lvert e_{i,j,k}\rvert}{2h_1h_3}$	$\frac{\lvert b_{i+1,j+1,k}\rvert + b_{i+1,j+1,k}}{4h_1h_2}$ $+ \frac{\lvert b_{i,j,k}\rvert + b_{i,j,k}}{4h_1h_2}$
j	$\frac{a_{i-1,j,k}+a_{i,j,k}}{2h_1^2}$ $- \frac{\lvert b_{i-1,j,k}\rvert + \lvert b_{i,j,k}\rvert}{2h_1h_2}$ $- \frac{\lvert c_{i-1,j,k}\rvert + \lvert_{i,j,k}\rvert}{2h_1h_3}$	$- \frac{a_{i-1,j,k}+2a_{i,j,k}+a_{i+1,j,k}}{2h_1^2}$ $- \frac{d_{i,j-1,k}+2d_{i,j,k}+d_{i,j+1,k}}{2h_2^2}$ $- \frac{f_{i,j,k-1}+2f_{i,j,k}+f_{i,j,k+1}}{2h_3^2}$ $- \frac{\lvert b_{i-1,j+1,k}\rvert - b_{i-1,j+1,k} + \lvert b_{i+1,j+1,k}\rvert + b_{i+1,j+1,k}}{4h_1h_2}$ $- \frac{\lvert b_{i-1,j-1,k}\rvert + b_{i-1,j-1,k} + \lvert b_{i+1,j-1,k}\rvert - b_{i+1,j-1,k}}{4h_1h_2}$ $+ \frac{\lvert b_{i-1,j,k}\rvert + \lvert b_{i+1,j,k}\rvert + \lvert b_{i,j-1,k}\rvert + \lvert b_{i,j+1,k}\rvert + 2\lvert b_{i,j,k}\rvert}{2h_1h_2}$ $- \frac{\lvert c_{i-1,j,k+1}\rvert - c_{i-1,j,k+1} + \lvert c_{i+1,j,k+1}\rvert + c_{i+1,j,k+1}}{4h_1h_3}$ $- \frac{\lvert c_{i-1,j,k-1}\rvert + c_{i-1,j,k-1} + \lvert c_{i+1,j,k-1}\rvert - c_{i+1,j,k-1}}{4h_1h_3}$ $+ \frac{\lvert c_{i-1,j,k}\rvert + \lvert c_{i+1,j,k}\rvert + \lvert c_{i,j,k-1}\rvert + \lvert c_{i,j,k-1}\rvert + 2\lvert c_{i,j,k}\rvert}{2h_1h_3}$ $- \frac{\lvert e_{i,j-1,k+1}\rvert - e_{i,j-1,k+1} + \lvert e_{i,j+1,k+1}\rvert + e_{i,j+1,k+1}}{4h_2h_3}$ $- \frac{\lvert e_{i,j-1,k-1}\rvert + e_{i,j-1,k-1} + \lvert e_{i,j+1,k-1}\rvert - e_{i,j+1,k-1}}{4h_2h_3}$ $+ \frac{\lvert e_{i,j-1,k}\rvert + \lvert e_{i,j+1,k}\rvert + \lvert e_{i,j,k-1}\rvert + \lvert e_{i,j,k+1}\rvert + 2\lvert e_{i,j,k}\rvert}{2h_2h_3}$	$\frac{a_{i+1,j,k}+a_{i,j,k}}{2h_1^2}$ $- \frac{\lvert b_{i+1,j,k}\rvert + \lvert b_{i,j,k}\rvert}{2h_1h_2}$ $- \frac{\lvert c_{i+1,j,k}\rvert + \lvert c_{i,j,k}\rvert}{2h_1h_3}$
j-1	$\frac{\lvert b_{i-1,j-1,k}\rvert + b_{i-1,j-1,k}}{4h_1h_2}$ $+ \frac{\lvert b_{i,j,k}\rvert + b_{i,j,k}}{4h_1h_2}$	$\frac{d_{i,j-1,k}+d_{i,j,k}}{2h_2^2} - \frac{\lvert b_{i,j-1,k}\rvert + \lvert b_{i,j,k}\rvert}{2h_1h_2} - \frac{\lvert e_{i,j-1,k}\rvert + \lvert e_{i,j,k}\rvert}{2h_1h_3}$	$\frac{\lvert b_{i+1,j-1,k}\rvert - b_{i+1,j-1,k}}{4h_1h_2}$ $+ \frac{\lvert b_{i,j,k}\rvert - b_{i,j,k}}{4h_1h_2}$
	i-1	i	i+1

k+1

j+1		$\frac{\lvert e_{i,j+1,k+1}\rvert + e_{i,j+1,k+1}}{4h_2h_3}$ $+ \frac{\lvert e_{i,j,k}\rvert + e_{i,j,k}}{4h_2h_3}$	
j	$\frac{\lvert c_{i-1,j,k+1}\rvert - c_{i-1,j,k+1}}{4h_1h_3}$ $+ \frac{\lvert c_{i,j,k}\rvert - c_{i,j,k}}{4h_1h_3}$	$\frac{f_{i,j,k+1}+f_{i,j,k}}{2h_3^2} - \frac{\lvert c_{i,j,k+1}\rvert + \lvert c_{i,j,k}\rvert}{2h_1h_3} - \frac{\lvert e_{i,j,k+1}\rvert + \lvert e_{i,j,k}\rvert}{2h_2h_3}$	$\frac{\lvert c_{i+1,j,k+1}\rvert + c_{i+1,j,k+1}}{4h_1h_3}$ $+ \frac{\lvert c_{i,j,k}\rvert + c_{i,j,k}}{4h_1h_3}$
j-1		$\frac{\lvert e_{i,j-1,k+1}\rvert - e_{i,j-1,k+1}}{4h_2h_3}$ $+ \frac{\lvert e_{i,j,k}\rvert - e_{i,j,k}}{4h_2h_3}$	
	i-1	i	i+1

Table 4. 3D Non-negative Stencil; This stencil is obtained by extending Weickert's 2D non-negative stencil to 3D. The stencil elements are non-negative as long as conditions of Equation 14 are satisfied, which results in a stable discretization.